archaeometry

Archaeometry ••, •• (2016) ••–•• doi: 10.1111/arcm.12232

CONFOCAL X-RAY FLUORESCENCE IMAGING FACILITATES HIGH-RESOLUTION ELEMENTAL MAPPING IN FRAGILE ARCHAEOLOGICAL BONE*

S. CHOUDHURY,[1] T. SWANSTON,[2] T. L. VARNEY,[3] D. M. L. COOPER,[4] G. N. GEORGE,[1] I. J. PICKERING,[1] V. GRIMES,[5] B. BEWER[6] and I. COULTHARD[6]†

[1]*Department of Geological Sciences, University of Saskatchewan, Saskatoon, Saskatchewan, S7N 5E2, Canada*
[2]*Department of Archaeology and Anthropology, University of Saskatchewan, Saskatoon, Saskatchewan, S7N 5B1, Canada*
[3]*Department of Anthropology, Lakehead University, Thunder Bay, Ontario, P7B 5E1, Canada*
[4]*Department of Anatomy and Cell Biology, University of Saskatchewan, Saskatoon, Saskatchewan, S7N 5E5, Canada*
[5]*Department of Archaeology, Memorial University, St. John's, Newfoundland and Labrador, A1C 5S7, Canada*
[6]*BioXAS, Canadian Light Source Inc., Saskatoon, Saskatchewan, S7N 2V3, Canada*

Synchrotron-based standard X-ray fluorescence imaging can be a sophisticated tool for mapping distributions of trace elements in archaeological bone; however, thin samples are normally required to achieve high-spatial-resolution results. Poorly preserved or fragile archaeological samples can be challenging to measure using this standard technique, since the production of a sufficiently thin section may be difficult. We discuss the implementation of confocal X-ray fluorescence imaging as a successful strategy for high-resolution elemental mapping in poorly preserved archaeological bone. The implementation of the confocal method additionally can facilitate localized quantification and speciation of elements, which are also discussed.

KEYWORDS: ANTIGUA, *C.* AD 1793–1822, BONE, SYNCHROTRON, CONFOCAL X-RAY FLUORESCENCE IMAGING, ELEMENTAL MAPPING, LEAD, BIOGENIC UPTAKE, DIAGENESIS

INTRODUCTION

The study of the trace elements in archaeological bone samples can provide insight into diet, environmental exposure and other determinants of health in the past (Rasmussen *et al*. 2008; Lanzirotti *et al*. 2014). The uptake of trace elements into bone microstructures through continuous remodelling during life makes bone a dynamic reservoir of trace elements. Since the elemental distribution in bone microstructures carries information about the temporal history of trace element deposition, our ability to extract such information enables us to potentially comment on lifestyle, health and diet of a subject. In particular, secondary osteons, also known as Haversian systems, are important structural units of bone where elemental deposition occurs (Martin *et al*. 2007). The 'secondary' status of these structures is a reference to the fact that they replace existing bone and thus provide a window on changes that occur even after growth of the skeleton is completed. Secondary osteons are roughly cylindrical microstructures oriented along the long axis of bone, comprising concentric layers, called lamellae, surrounding a central canal that provides housing for blood vessels and nerves. The deposition of trace elements that occurs during life, referred to as biogenic uptake, is our key interest for extracting information about life history. However, *post-mortem* contamination due to leaching of trace elements from the burial environment, referred to as diagenesis, constitutes a confounding factor for this area of research.

*Received 10 June 2015; accepted 10 November 2015
†Corresponding author: email ian.coulthard@lightsource.ca

In order for an accurate reconstruction of the lifestyle of a subject, diagenesis needs to be addressed prior to the use of data (Zapata *et al*. 2006). High-resolution maps of elemental distribution are thus essential to the analysis of the incorporation of elements in bone microstructures.

Experimental techniques commonly applied to study trace elements in archaeological bone samples include: laser ablation inductively coupled plasma mass spectrometry (LA–ICP–MS) (Koenig *et al*. 2009; Kohn and Moses 2013); atomic absorption spectrophotometry (AAS) (Arnay-de-la-Rosa *et al*. 1998; Arnay-de-la-Rosa *et al*. 2011); scanning electron microscopy (SEM) (Freestone *et al*. 1987; Bell 1990); and synchrotron-based X-ray fluorescence imaging (XFI) (Kanngießer *et al*. 2003; Grolimund *et al*. 2004; Martin *et al*. 2007, 2013; Bertrand *et al*. 2011; Swanston *et al*. 2012; Pemmer *et al*. 2013). While useful, techniques such as LA–ICP–MS and AAS are inherently destructive in nature. Depending on the elemental concentration in a sample, AAS may require substantially more sample than is generally available from fragile archaeological samples. Although SEM is considered non-destructive, it is limited to surface characterization and involves extensive sample preparation. Synchrotron-based standard XFI is a powerful tool for non-invasive investigation of elemental distribution with minimal sample preparation; fundamentals of the technique can be found elsewhere (Pushie *et al*. 2014). While thick samples can in fact be measured, high-resolution results showing the incorporation of elements in microstructures are acquired in standard XFI only from very thin samples (Vekemans *et al*. 2004). The use of a thick sample (e.g., a ground bone section) results in a blurry image due to the superposition of fluorescence originating from features at a range of depths within the sample (Wittmers *et al*. 2008). Swanston *et al*. reported an application of standard XFI by utilizing archaeological bone sections carefully ground down to ~100 μm thickness (Swanston *et al*. 2012). However, preparing a section of micron-scale thickness from an archaeological bone may not always be feasible due to the state of preservation of the sample. Besides, archaeological samples are often valuable, necessitating minimum processing. Therefore, there is an increasing demand for non-invasive techniques for elemental analysis that improve spatial resolution while minimizing both sample quantity and sample preparation.

In this study, we apply the synchrotron-based confocal XFI technique (Janssens *et al*. 2004; Woll *et al*. 2006) to determine the spatial elemental distribution in archaeological bone samples obtained from several different sites, the most prominent being the Royal Naval Hospital cemetery (*c*. ad 1793–1822) near English Harbour, Antigua. Historical sources indicate that this hospital provided care to British military personnel and the surrounding general populace during the Napoleonic Wars, wherein the British suffered huge losses due to tropical diseases and other illnesses (Varney and Nicholson 1999). Lead (Pb) contamination is believed to have contributed to the demise of the British military, since Pb was commonly present in eating and cooking utensils, water catchment systems and alcohol distillation equipment in that era (Varney and Nicholson 1999; Varney *et al*. 2012). For these reasons, we have chosen Pb as a representative element to demonstrate the efficacy of this imaging technique, although other archeologically and biologically important trace elements such as calcium, zinc, strontium, barium and bromine can also be measured simultaneously following the described methodology. The implementation of confocal XFI not only avoids physical thin sectioning of the sample but also produces elemental maps showing accumulation of Pb in bone microstructures with excellent detail. A comparison between standard and confocal XFI results is presented to demonstrate the advantage of the confocal method. The resultant high resolution is due to confocal detection, which facilitates not only optical sectioning of sample but also superior rejection of scatter. Synchrotron-based confocal XFI can be a valuable addition to the toolkits of bioarchaeologists, especially in unravelling elemental distribution within fragile samples.

MATERIALS AND METHODS

Samples

Four bone samples were analysed from three distinct sites in three different countries. Table 1 describes, by name, location and sample name, the sites analysed using this technique in this study.

The most prominent site in terms of the number of available samples was the Royal Naval Hospital cemetery (*c*. ad 1793–1822) near English Harbour, Antigua. Samples were recovered during the mitigation of the cemetery due to encroachment by modern construction. Ethics approval was obtained from the University of Saskatchewan Biomedical Research Ethics Board for all samples prior to analysis. Samples were specifically chosen for this study representing different sites with very different burial environments, soil conditions and weather, in order to demonstrate the efficacy of this technique regardless of variances in these factors. All bones utilized were long bones such as fibula and ulna, with outer cortical layers and similar microstructural features.

ICP–MS

Initial testing of the samples included a bulk analysis of the lead concentrations using standard methodologies at the ICP–MS Laboratory in the Department of Geological Sciences at the University of Saskatchewan (Swanston *et al*. 2012). Quality control standard BCR-2 shows that the long-term analytical error for Pb is ±7%.

Standard XFI

Experiments were carried out at the 20ID-B (PNC/XSD) beamline of the Advanced Photon Source (APS) at the Argonne National Laboratory (Illinois, USA), with the storage ring operating in continuous top-up mode at 102 mA and 7.0 GeV. The incoming beam was tuned to the desired excitation energy of 16.5 keV (with an estimated intensity of ~10^{12} photons per second) by using a liquid-nitrogen-cooled Si (111) double crystal monochromator, with a second crystal detuned by 15% to reduce harmonic contamination. A micro-beam of approximately 5 × 5 μm spot-size was produced using Rh-coated silicon Kirkpatrick–Baez (K–B)–style focusing mirrors, which also served to provide additional harmonic rejection. Samples were mounted on a motorized stage at 45° to the incident beam. The Pb–Lα fluorescent emission lines at 10.55 and 10.44 keV and other fluorescence X-rays were monitored using a Si-drift Vortex® detector

Table 1 *Samples analysed using confocal XFI, arranged by site name and site location*

Site name	*Site location*	*Name of sample*	*Approximate thickness of sample (μm)*
Royal Naval Hospital Cemetery	English Harbour, Antigua	B3	140 (non-confocal) 1980 (confocal)
Royal Naval Hospital Cemetery	English Harbour, Antigua	B18	450 (confocal)
Harney Site	Montserrat	H1	1550 (confocal)
South Side Naval Cemetery	Newfoundland, Canada	R4NL	680 (confocal)

(SII NanoTechnology USA Inc.) placed at 90° with respect to the incident X-ray beam in the horizontal plane. An ionization chamber monitored the intensity of the incident X-ray beam, I_0, which was used for the normalization of the fluorescence; this process eliminates the impact of any possible flux variations of the source.

Confocal XFI

Confocal XFI experiments were also carried out at the 20ID-B (PNC/XSD) beamline with the following modifications. To create the confocal geometry, an additional focusing optic, a polycapillary (XOS®) of nominal 25 μm diameter focal spot (at Mo–Kα; 17.4 keV), was installed in front of the Si-drift Vortex® detector. Figure 1 shows a schematic diagram and a photograph of the confocal XFI experiment at 20ID-B, APS. The arrangement for a standard XFI experiment differed only in the absence of the polycapillary, which is not required for the standard technique. The sample was positioned at an orientation of 45° to both the incident X-ray beam and detector, with the detector at 90° to the incident beam in order to minimize the inelastic scattering of linearly polarized synchrotron radiation, as the scattering cross-section along the **e**-vector is zero (Haller and Knochel 1996). Figure 1 shows: (1) the Kirkpatrick–Baez (K–B) mirror—a focusing optic on the incident beam to produce a micro-focused beam; (2) the ionization chamber I_0—a unit that measures incident beam intensity; (3) the sample stage—a platform that holds the sample and allows its *XYZ* translation; (4) the detector—an energy-dispersive fluorescence detector that measures fluorescence emitted from the sample; and (5) the polycapillary—a second focusing optic on the detection side, for confocal detection. Figure 1 (a) schematically shows the formation of confocal volume (*Vc*) within the sample.

Data analysis

Data from both experimental configurations were analysed using the SMAK software package (http://home.comcast.net/~sam_webb/smak.html). The recorded fluorescence counts were normalized to the incident intensity I_0 (Figure 1) and were background corrected by subtracting the average intensity of pixels outside the image from the intensity of each pixel of the image.

Quantification was performed by first normalizing the sample measurement to the known reference material with respect to incident photon flux, dwell time and detector sensitivity. Sample fluorescence signal loss from absorption due to confocal depth within the sample was corrected for by using the known surface calcium count rate, compared to the count rate measured at each point to determine the local depth for each pixel. The measured Pb count rate for the reference material could then be compared to the measured Pb count rate for the sample; and using the known concentration of the reference, the sample concentration was determined (Bewer 2015).

RESULTS AND DISCUSSION

A small portion of certain samples was sacrificed for the ICP–MS measurement, which determined the bulk levels of Pb in samples B3 and B18 to be 75 and 58 ppm, respectively. The amount of material sacrificed was approximately 0.05–0.1 g by weight and was always taken from a section of bone immediately adjacent to the section of bone analysed with XRF. While the presence of Pb in bone may indicate that the subject was exposed to Pb while living, diagenesis could also be the source of Pb. Quantification of the lead levels using the confocal XFI image for sample B18 (Bewer 2015) yielded whole-bone Pb concentration levels consistent with the

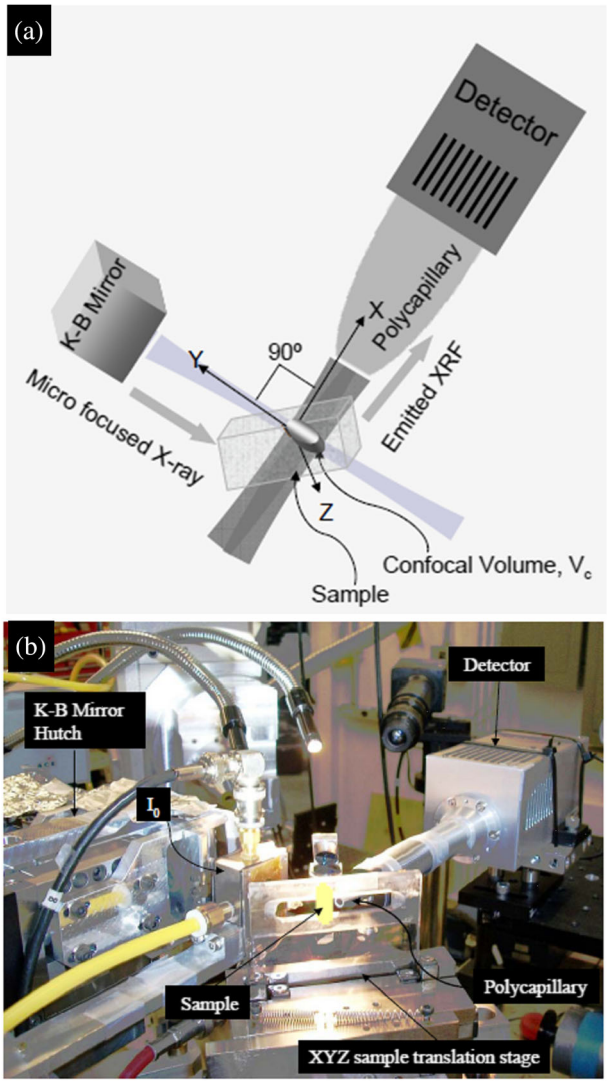

Figure 1 *The confocal XFI arrangement at beamline 20ID-B, APS, shown as (a) a schematic diagram and (b) a photograph. The sample is at 45° to the incident beam and detector. The schematic diagram shows the formation of the confocal volume (Vc) within the sample through the intersection of foci of incident and detection focusing optics (K–B mirror and polycapillary, respectively). The sample can be rastered along XYZ directions through Vc to produce elemental maps along desired planes.*

ICP–MS level, though typically 10–25% lower. Of greater interest is the ability to glean localized Pb concentration methods from this method. The quantification method yielded localized maxima of Pb concentrations of several hundreds of ppm at the canal walls of some osteons, with the highest observed localized concentration being ~600 ppm.

In a standard XFI experiment, which lacks a focusing optic on the detector, the fluorescence emitted from the range of sample depths interrogated by the incident beam is collected directly by the detector. Mapping is accomplished by rastering the area of interest through the incident

micro-beam with simultaneous measurement of fluorescence. Since the fluorescence lines of elements are at well-defined energies, this technique offers excellent element specificity. However, although standard XFI is a widely used technique for elemental mapping, it is not designed to discriminate information originating from different depths within the sample. The fluorescences emitted from microstructures at a range of depths are detected and superposed on a two-dimensional map, resulting in a blurry image. In order to minimize this problem, the thickness of sample used for the standard XFI measurement can be reduced by physical sectioning. However, preparation of thin sections is frequently not possible; for example, sample B18 in this study was deemed to be too fragile to be sectioned. We therefore have employed confocal XFI to accomplish elemental mapping in sample B18.

Figure 2 represents Pb elemental maps obtained from sample B3 by employing standard (Fig. 2 (a)) and confocal XFI (Fig. 2 (b)), respectively. Two separate pieces of sample B3 were utilized, one thinned to 140 μm of thickness and the other left intact, with a thickness of 1980 μm. A ~2 × 2 mm area of interest from each piece of sample B3 was mapped with a 20 μm step-size, where each mapping took approximately 2.5 h. The comparison between standard- and confocal-derived maps in this figure demonstrates that confocal XFI (Fig. 2 (b)) yields an elemental map with significantly improved spatial resolution compared with standard XFI (Fig. 2 (a)), showing excellent details of the incorporation of Pb in various bone microstructures. Structural detail observed in the confocal map (Fig. 2 (b)) includes younger osteons, older osteons, cement lines and osteonal canals. A younger osteon can be identified as a continuous closed-ring structure with a central canal, whereas an older osteon appears as a discrete broken-ring structure with or without a central canal formed during regular bone tissue maintenance or turnover. The osteonal canals are easily identified as holes at the centre of the osteons. Cement lines are observed as the boundary lines of osteons, with some broken cement lines observed as the remnants of old osteons.

Figure 2 shows clear accumulation of Pb in bone microstructures but no accumulation in the periosteal surfaces (the right sample surface in Fig. 2 (b)), which are the outer surfaces of the bone fragment that were most directly exposed to the burial environment. Pb is observed in most canal walls and cement lines, while few osteons show Pb enrichment throughout the entire

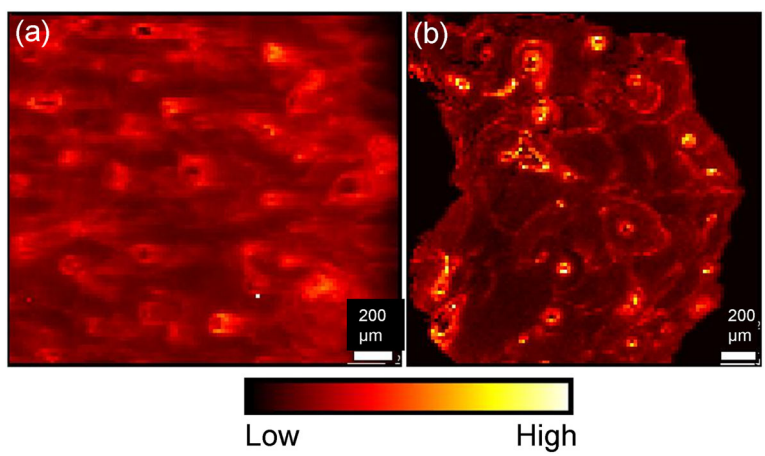

Figure 2 *X-ray fluorescence maps showing the Pb distribution in bone microstructures: 2 × 2 mm areas of (a) sample B3 measured using standard mode and (b) sample B3 measured using confocal mode. Comparison between (a) and (b) demonstrates the advantage of confocal XFI in generating high-resolution elemental maps from fragile archaeological bone. The intensity scale shows the relative amounts of Pb from black (lowest Pb) through varying intensity of colouration to white (highest Pb).*

structure. Although most canals show clear Pb accumulation, a few show little or no accumulation at all. These results are consistent with previous results on archaeological bone (Swanston *et al*. 2012), where such patterns of lead were attributed to be indicative of biogenic uptake. They are also strikingly similar to results (Pemmer *et al*. 2013) where the samples were modern bone from cadavers that had not been exposed to a burial environment and the subsequent diagenetic factors.

In comparison, Figure 2 (a) shows a standard XFI map obtained from sample B3. Clearly, the spatial resolution in this map is considerably degraded compared to the confocal one. The three-dimensional (3D) structure of osteons, comprising cylindrical structures of varying diameter and 3D angular orientation arranged throughout the depth of sample, explains the blurred appearance of the map. If an irregular 3D structure is viewed using a standard imaging technique, the resulting image is a juxtaposition of fluorescence from different features situated at different depths within the sample. While some 3D information, such as the angular orientation of the cylindrical structures in the sample, might be extractable from such an image, the ability to resolve individual features is significantly reduced. This map (Fig. 2 (a)) thus demonstrates the challenge of employing standard XFI in investigating an irregular 3D feature within a thicker sample, which is significantly improved using confocal detection in Figure 2 (b).

Figure 3 shows confocal images of sample B18 for multiple elements taken simultaneously, demonstrating that while the emphasis in this paper has been on showing lead accumulation images, the power of the energy-dispersive type detector used means that the fluorescence signals from all of the elements within the sample are analysed at the same time. This makes this data available for all elements and all samples, and also assures that all maps of the full set of elements overlap each other without offset. The position of the confocal focusing optic relative to the sample and the detector also assures that all images for the full set of elements are confocal images. Figure 4 shows lead confocal XFI images for a pair of samples (H1 and R4NL) from different locations other than the Naval Hospital Site in Antigua, demonstrating that the technique works perfectly well for samples taken from a diverse variety of locations and burial conditions, and is not only applicable to a narrow set of samples collected or found under ideal or extremely specific conditions.

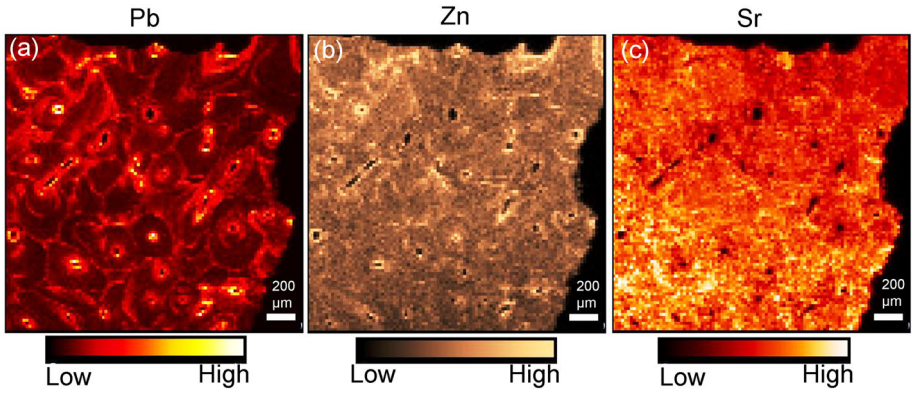

Figure 3 *X-ray fluorescence maps showing the distribution of (a) Pb, (b) Zn and (c) Sr in bone microstructures of sample B18. The scan size is 2 × 2 mm. In all images, the intensity scale shows the relative amounts of the elements, with the darkest colouration being the lowest amounts and the lightest colouration being higher, with white being the highest.*

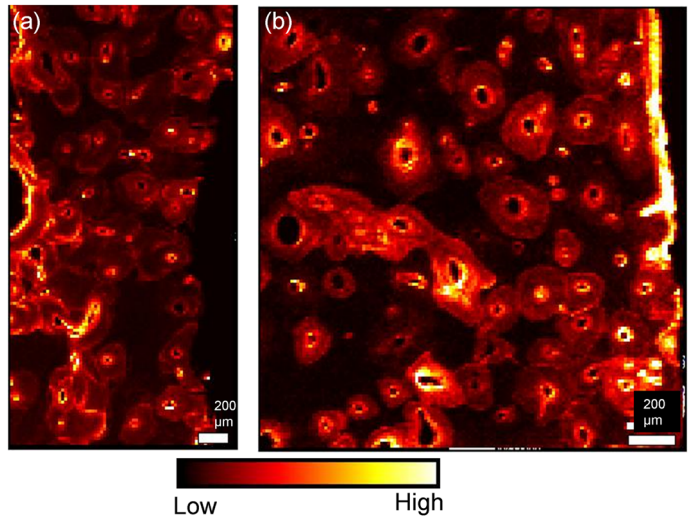

Figure 4 *X-ray fluorescence maps showing the distribution of Pb in the bone microstructures of samples (a) R4NL and (b) H1. The scan sizes are ~2 × 2 mm but were slightly modified to account for sample shape. In all images, the intensity scale shows the relative amounts of Pb, with the darkest colouration being the lowest amounts and the lightest colouration being higher, with white being the highest.*

In confocal XFI experiments, excitation and detection coincide only at the intersecting volume, commonly known as the confocal volume, defined by the foci of the incident (K–B mirror) and detection (polycapillary) focusing optics. Since the focal spot of the polycapillary (25 µm diameter at the Mo–Kα energy) is much larger than the beam spot size (5 × 5 µm), the resulting detection volume would be ellipsoidal (Silversmit *et al*. 2010) with approximate dimensions of $40 \times 5 \times 5\ \mu m^3$ (Silversmit *et al*. 2010) at the energy of Pb–L*α*. Elemental maps can be obtained by spatially rastering the sample through the confocal volume along any desired plane within the sample. This technique therefore removes the need for physical sectioning of sample through its inherent ability of optical sectioning. Implementation of the confocal technique also greatly helps to improve the signal-to-noise ratio in the resulting maps due to the collimating nature of polycapillary, since fluorescent and scattered photons are collected essentially only from the volume of interest (Wilke *et al*. 2010). In comparison, a standard XFI experiment will show a much larger scatter peak as the detector collects fluorescence from a much longer intersection path of the beam through the sample (limited by the absorption length). Besides, as the detection solid angle in a standard XFI experiment is much larger compared to the confocal, scatter originated from other sources such as mounts, windows, air or other gas and other beamline equipment may also be detected. A superior signal-to-noise ratio is particularly important for the detection of low-concentration elements in the sample. Further, this optical form of sectioning clearly gives better results in terms of co-localizing the elements to the microstructural features of the bone.

The variation in Pb accumulation in bone microstructures may carry significant information regarding health, lifestyle or diagenesis. However, a detailed observation of the incorporation of Pb throughout the various components of bone microstructures is necessary in order to be able to comment on what might be the underlying reason for such variations. We emphasize here the potential of confocal XFI in producing high-resolution maps that will make such observation possible. Additionally, a high-resolution confocal map may exclude the need for a matching histological image, which was necessary for the interpretation of a standard XFI map in a previous study (Swanston *et al*. 2012).

Another important advantage of employing confocal XFI is its ability to make X-ray absorption spectroscopy (XAS) possible for an element of interest within a very specific detection volume from within the sample, allowing assessment of the localized chemical form of elements (Silversmit *et al*. 2010). Confocal XAS may thus aid in differentiating between the biogenic and diagenetic nature of elements in archaeological samples by looking for differences in speciation of elements at specific structural features of the bone such as: osteon canal wall, cement line and periosteal surface. Moreover, localized quantitative information about the elements is available from confocal XFI maps given that self-absorption of incident and fluorescent X-rays can be estimated (De Samber *et al*. 2010; Bewer 2015). Quantitative elemental analysis may aid in the differentiation of acute or chronic exposure to toxic elements. Further improvements in the spatial resolution of confocal XFI can be achieved by implementing a novel detection focusing optic, a micro-channel array (Woll *et al*. 2014). We intend to explore this potential in future studies.

CONCLUSIONS

This paper demonstrates the potential of synchrotron-based confocal XFI as a tool to generate high-spatial-resolution elemental maps from fragile archaeological bone samples showing excellent details of elemental incorporation into bone microstructures. Fragile or poorly preserved archaeological samples cannot be processed to create sufficiently thin sections for elemental mapping using standard XFI experiments. Confocal XFI, which inherently produces optical sections, avoids the need for physical sectioning. Besides enabling optical sectioning, the confocal mode also aids in generating maps of a higher signal-to-noise ratio by considerably reducing the background scatter. This technique should help elucidate the origins of observed elements in the bone samples, and whether they are biogenic, diagenetic or a combination of both.

ACKNOWLEDGEMENTS

This research was supported by a Social Sciences and Humanities Research Council (SSHRC) Insight Development Grant (#430-2012-0236), by NSERC Discovery Grants (to GNG and IJP), and by the Canada Foundation of Innovation through funding for BioXAS: Life Science Beamline for X-ray Absorption Spectroscopy at the Canadian Light Source Inc. SC is a fellow in the Canadian Institutes of Health Research Training grant in Health Research Using Synchrotron Techniques (CIHR-THRUST, IJP and others). GNG, IJP and DMLC are Canada Research Chairs. This work was also supported by the Canadian Foundation of Innovation through funding for BioXAS: Life Science Beamline for X-ray Absorption Spectroscopy at the Canadian Light Source Inc. PNC/XSD 20-ID-B. PNC/XSD facilities at the Advanced Photon Source (APS) are supported by the US Department of Energy (DOE)—Basic Energy Sciences, the Canadian Light Source and its funding partners, the University of Washington and the APS. The use of the APS was supported by the US Department of Energy, Office of Science, Office of Basic Energy Sciences, under Contract No. DE-AC02-06CH11357.

REFERENCES

Arnay-de-la-Rosa, M., Gonzalez-Reimers, E., Velasco-Vazquez, J., Barros-Lopez, N., and Galindo-Martin, L., 1998, Bone trace element pattern in an 18th century population sample of Tenerife (Canary Islands): comparison with a prehistoric one, *Biological Trace Element Research*, **65**, 45–51.

Arnay-de-la-Rosa, M., González-Reimers, E., Yanes, Y., Romanek, C. S., Noakes, J. E., and Galindo-Martín, L., 2011, Paleonutritional and paleodietary survey on prehistoric humans from Las Cañadas del Teide (Tenerife, Canary Islands) based on chemical and histological analysis of bone, *Journal of Archaeological Science*, **38**, 884–95.

Bell, L. S., 1990, Palaeopathology and diagenesis: an SEM evaluation of structural changes using backscattered electron imaging, *Journal of Archaeological Science*, **17**, 85–102.

Bertrand, L., Robinet, L., Thoury, M., Janssens, K., Cohen, S. X., and Schöder, S., 2011, Cultural heritage and archaeology materials studied by synchrotron spectroscopy and imaging, *Applied Physics A*, **106**, 377–96.

Bewer, B., 2015, Quantification estimate methods for synchrotron radiation X-ray fluorescence spectroscopy, *Nuclear Instruments and Methods in Physics Research B*, **347**, 1–6.

De Samber, B., Silversmit, G., De Schamphelaere, K., Evens, R., Schoonjans, T., Vekemans, B., Janssen, C., Masschaele, B., Van Hoorebeke, L., Szalóki, I., Vanhaecke, F., Rickers, K., Falkenberg, G., and Vincze, L., 2010, Element-to-tissue correlation in biological samples determined by three-dimensional X-ray imaging methods, *Journal of Analytical Atomic Spectrometry*, **25**, 544–53.

Freestone, I. C., Middleton, A. P., and Museum, B., 1987, Mineralogical applications of the analytical SEM in archaeology, *Mineralogical Magazine*, **51**, 21–31.

Grolimund, D., Senn, M., Trottmann, M., Janousch, M., Bonhoure, I., Scheidegger, A. M., and Marcus, M., 2004, Shedding new light on historical metal samples using micro-focused synchrotron X-ray fluorescence and spectroscopy, *Spectrochimica Acta Part B*, **59**, 1627–35.

Haller, M., and Knochel, A., 1996, X-ray fluorescence analysis using synchrotron radiation (SYXRF), *Journal of Trace and Microprobe Techniques*, **14**, 461–88.

Janssens, K., Proost, K., and Falkenberg, G., 2004, Confocal microscopic X-ray fluorescence at the HASYLAB microfocus beamline: characteristics and possibilities, *Spectrochimica Acta Part B*, **59**, 1637–45.

Kanngießer, B., Malzer, W., and Reiche, I., 2003, A new 3D micro X-ray fluorescence analysis set-up – first archaeometric applications, *Nuclear Instruments and Methods in Physics Research B*, **211**, 259–64.

Koenig, A. E., Rogers, R. R., and Trueman, C. N., 2009, Visualizing fossilization using laser ablation – inductively coupled plasma – mass spectrometry maps of trace elements in Late Cretaceous bones, *Geology*, **37**, 511–4.

Kohn, M. J., and Moses, R. J., 2013, Trace element diffusivities in bone rule out simple diffusive uptake during fossilization but explain *in vivo* uptake and release, *Proceedings of the National Academy of Sciences of the United States of America*, **110**, 419–24.

Lanzirotti, A., Bianucci, R., LeGeros, R., Bromage, T. G., Giuffra, V., Ferroglio, E., Fornaciari, G., and Appenzeller, O., 2014, Assessing heavy metal exposure in Renaissance Europe using synchrotron microbeam techniques, *Journal of Archaeological Sciences*, **52**, 204–17.

Martin, R. R., Naftel, S. J., Nelson, A. J., and Sapp, D. W. III, 2007, Comparison of the distributions of bromine, lead, and zinc in tooth and bone from an ancient Peruvian burial site by X-ray fluorescence, *Canadian Journal of Chemistry*, **85**, 831–6.

Martin, R. R., Naftel, S., Macfie, S., Jones, K., and Nelson, A., 2013, Pb distribution in bones from the Franklin expedition: synchrotron X-ray fluorescence and laser ablation/mass spectroscopy, *Applied Physics A*, **111**, 23–9.

Pemmer, B., Roschger, A., Wastl, A., Hofstaetter, J. G., Wobrauschek, P., Simon, R., Thaler, H. W., Roschger, P., Klaushofer, K., and Streli, C., 2013, Spatial distribution of the trace elements zinc, strontium and lead in human bone tissue, *Bone*, **57**, 184–93.

Pushie, M. J., Pickering, I. J., Korbas, M., Hackett, M. J., and George, G. N., 2014, Elemental and chemically specific X-ray fluorescence imaging of biological systems, *Chemical Reviews*, **114**, 8499–541.

Rasmussen, K. L., Boldsen, J. L., Kristensen, H. K., Skytte, L., Hansen, K. L., Mølholm, L., Grootes, P. M., Nadeau, M.-J., and Eriksen, K. M. F., 2008, Mercury levels in Danish medieval human bones, *Journal of Archaeological Science*, **35**(8), 2295–306.

Silversmit, G., Vekemans, B., Nikitenko, S., Schmitz, S., Schoonjans, T., Brenker, F. E., and Vincze, L., 2010, Spatially resolved 3D micro-XANES by a confocal detection scheme, *Physical Chemistry Chemical Physics*, **12**, 5653–9.

Swanston, T., Varney, T., Coulthard, I., Feng, R., Bewer, B., Murphy, R., Hennig, C., and Cooper, D., 2012, Element localization in archaeological bone using synchrotron radiation X-ray fluorescence: identification of biogenic uptake, *Journal of Archaeological Science*, **39**, 2409–13.

Varney, T. L., and Nicholson, D. V., 1999, Digging the 'Grave of the Englishman': a preliminary report on excavations at a former British navy hospital cemetery, English Harbour, Antigua, WI, in *Proceedings of the XVIII International Congress for Caribbean Archaeology, Grenada, WI*, 329–35, Association Internationale d'Archéologie de la Caraïbe, Basse Terre, Guadaloupe (F.W.I).

Varney, T. L., Swanston, T., Coulthard, I., Cooper, D. M. L., George, G. N., Pickering, I. J., and Murphy, A. R., 2012, A preliminary investigation of lead contamination in a Napoleonic era naval cemetery in Antigua, W.I, in *Caribbean connections: a publication of the Field Research Centre 2(1): special issue focusing in the bioarchaeology of the Caribbean*, II(1); http://fieldresearchcentre.weebly.com/index.html

Vekemans, B., Vincze, L., Brenker, F. E., and Adams, F., 2004, Processing of three-dimensional microscopic X-ray fluorescence data, *Journal of Analytical Atomic Spectrometry*, **19**, 1302–8.

Wilke, M., Appel, K., Vincze, L., Schmidt, C., Borchert, M., and Pascarelli, S., 2010, A confocal set-up for micro-XRF and XAFS experiments using diamond-anvil cells, *Journal of Synchrotron Radiation*, **17**, 669–75.

Wittmers, L. E., Aufderheide, A. C., Pounds, J. G., Jones, K. W., and Angel, J. L., 2008, Problems in determination of skeletal lead burden in archaeological samples: an example from the First African Baptist Church population, *American Journal of Physical Anthropology*, **136**, 379–86.

Woll, A. R., Mass, J., Bisulca, C., Huang, R., Bilderback, D. H., Gruner, S., and Gao, N., 2006, Development of confocal X-ray fluorescence (XRF) microscopy at the Cornell high energy synchrotron source, *Applied Physics A*, **83**, 235–8.

Woll, A. R., Agyeman-Budu, D., Choudhury, S., Coulthard, I., Finnefrock, A. C., Gordon, R., Hallin, E., and Mass, J., 2014, Lithographically-fabricated channel arrays for confocal x-ray fluorescence microscopy and XAFS, *Journal of Physics: Conference Series*, **493**012028, 1–4.

Zapata, J., Pérez-Sirvent, C., Martínez-Sánchez, M. J., and Tovar, P., 2006, Diagenesis, not biogenesis: two late Roman skeletal examples, *Science of the Total Environment*, **369**, 357–68.